Available online at www.sciencedirect.com
ScienceDirect
Physics Reports 448 (2007) 115–132
PHYSICS REPORTS
www.elsevier.com/locate/physrep

Isotropic and anisotropic electroconvection

Ágnes Buka[a,*], Nándor Éber[a], Werner Pesch[b], Lorenz Kramer[b]

[a] *Research Institute for Solid State Physics and Optics, Hungarian Academy of Sciences, H-1525 Budapest, P.O.B. 49, Hungary*
[b] *Institute of Physics, University of Bayreuth, D-95440 Bayreuth, Germany*

Available online 28 March 2007
editor: I. Procaccia

Abstract

A systematic overview of various electric-field induced pattern forming instabilities in nematic liquid crystals is given. The standard hydrodynamic description of nematics predicts the occurrence of striped patterns (rolls) in various wavenumber ranges, which depend on the anisotropy of the dielectric permittivity and that of the electrical conductivity as well as on the initial director orientation (planar or homeotropic). We discuss in detail three basic configurations with emphasis on the characterization of the threshold voltage and the critical wavenumber of the resulting patterns. Some features of the weakly nonlinear behavior are also addressed. Experimental exploration of additional pattern types, not captured by the standard model of electroconvection, is also presented. The impact of flexoelectricity as a possible explanation of the nonstandard EC patterns is discussed.

PACS: 47.54.+r; 61.30.Gd; 47.20.Ky; 78.20.Jq

Keywords: Electroconvection; Pattern; Nematic liquid crystal; Anisotropy

Contents

* Corresponding author. Tel.: +36 1 392 2217; fax: +36 1 392 2768.
E-mail address: ab@szfki.hu (Á. Buka).

0370-1573/$ - see front matter © 2007 Elsevier B.V. All rights reserved.
doi:10.1016/j.physrep.2007.02.013

1. Introduction

Pattern forming instabilities in macroscopic systems driven out of equilibrium by external stresses are common in nature and have intensely been studied over the last decades. Prominent examples are provided by fluid systems where the structures are typically associated with material flow [1]. The understanding of such systems has in particular benefitted from investigations on the classical buoyancy driven Rayleigh–Bénard convection (RBC) in a layer of a simple fluid heated from below [2]. Careful experiments which match very well the numerical results of the underlying hydrodynamic equations have been crucial for the development and the precise tests of the present standard concepts to characterize the many facets of convective pattern formation in nature. One typically starts from the linear stability analysis to capture the primary instability at onset which is followed by an amplitude equation approach to describe the saturation of the pattern amplitude in the weakly nonlinear regime. Then secondary and subsequent bifurcations are investigated which lead to increased complexity and eventually to chaos and turbulence.

Convection instabilities in more complex, anisotropic fluid systems—e.g. liquid crystals (LCs)—have also attracted considerable interest. In particular focus has been on the class of nematic LCs (nematics) which are liquids with a long-range uniaxial orientational ordering. The local symmetry axis is described by the director field $\mathbf{n}(\mathbf{r}, t)$ ($\mathbf{n}^2 = 1$), which responds elastically to distortions. The director orientation is sensitive to electric and magnetic fields, furthermore it is coupled via viscous torques to the flow field $\mathbf{v}(\mathbf{r}, t)$ [3].

The anisotropic properties of liquid crystals, especially the director-flow coupling, allow for novel, physically attractive convective destabilization mechanisms [4–6]. They have intensively been studied in electric-field induced convection (electroconvection, EC) in nematics [7–9], which has become a prominent paradigm for studying the generic features of *anisotropic* and recently also of *isotropic* convection. A crucial ingredient is here the initial symmetry of the convecting LC layer which can conveniently be chosen by the boundary conditions. In the case of a planar initial director alignment ($\mathbf{n}$ in the plane of the layer) the EC destabilization leads typically to a preferred orientation (anisotropy) of the pattern itself, a feature which is not easy to enforce in isotropic fluids. In the case of homeotropic director alignment where $\mathbf{n}$ is perpendicular to the layer resulting in a rotational symmetry in the plane, two scenarios can be distinguished. Depending on the material parameters one observes either a direct transition to EC patterns (in analogy to isotropic pattern formation) or EC occurs as a secondary instability upon a homogeneously distorted Freedericksz ground state which has a spontaneously broken rotational symmetry (quasi-anisotropy). In the latter case the system can be toggled between quasi-anisotropy and anisotropy by an additional magnetic field.

Studying EC in nematics has further appealing features. The large aspect ratio of the typical experimental cells allows the observation of extended regions with regular roll patterns on a convenient time scale. The patterns are easy to visualize by exploiting the birefringence of LCs. Furthermore the number of accessible control parameters is larger than in isotropic fluid convection. For instance, one can easily change the amplitude and the frequency of an applied ac voltage and/or apply a magnetic field. Even the amount of anisotropy can be altered by changing the distance in temperature to the nematic–isotropic phase transition.

From the theoretical point of view universal aspects of pattern formation can more easily be addressed in anisotropic systems since a Ginzburg–Landau (GL) type amplitude equation formalism can rigorously be justified only in the case of a preferred pattern orientation [10]. On the other hand isotropic pattern forming systems near onset are often assessed by Swift–Hohenberg models which are less well founded from first principles. In isotropic EC they yield in fact a surprisingly accurate description of the experiments [11]. Though the hydrodynamic description of liquid crystals may look prohibitively complex, in fact a quantitative description of experiments has been achieved in many cases. In general, one might state that liquid crystals have just the right amount and right kind of complexity and non-linearity to make them attractive but still tractable.

In this article we will concentrate on various aspects and on new developments in electroconvection of nematic liquid crystals. In Section 2 we sketch the essence of the standard model of EC which is based on the Carr–Helfrich (CH) mechanism. In the following sections the detailed discussion of EC is presented in the light of the director configuration in the ground state and of the sign of the anisotropy of the dielectric permittivity ϵ_a and that of the electrical conductivity σ_a. In Section 3 the situation will be discussed where EC occurs as a primary forward bifurcation in a planarly aligned cell (anisotropic EC). In addition we describe here the decay mechanism of the roll pattern. Then, in Section 4, we address the homeotropic configuration (quasi-anisotropic EC) where convection sets in as a secondary instability upon an already distorted Freedericksz ground state. We describe the effect of an additional magnetic field on the threshold and on the morphological transitions of EC, the abnormal rolls (AR) and the dynamics of defects. Next, in Section 5,

we describe the case where isotropic EC occurs as a primary forward bifurcation under homeotropic initial alignment. Section 6 is devoted to EC patterns occurring for material parameter combinations where the CH mechanism is ruled out. Finally, in Section 7, we present an outlook to electroconvection in liquid crystals with large flexoelectric polarization. The paper ends with some concluding remarks.

2. The standard (Carr–Helfrich) mechanism

Electroconvection is typically studied experimentally in sandwich cells, similar to those used for LC displays (a plane capacitor with transparent electrode plates parallel to the x–y plane), filled with a nematic. An ac voltage $U(t) = U_0 \cos(\omega t)$ is applied to the electrodes separated by a distance d $(-d/2 < z < d/2)$ which yields an electric field $\mathbf{E}$ across the layer (along the z axis). By a suitable surface treatment the director is aligned either parallel (planar configuration) or perpendicular (homeotropic configuration) to the confining electrodes in order to induce a homogeneous ground state for $U = 0$. The lateral extension (a few cm) of the cells is much larger than the cell gap ($d = 10$–$100\,\mu$m), providing a large aspect ratio.

At onset EC typically represents a regular array of convection rolls associated with a spatially periodic modulation of the director and a separation of space charges. The periodicity of the pattern in the x–y plane is characterized by the wave vector $\mathbf{q} = (q, p)$. One speaks of "normal" rolls if $\mathbf{q} \| \mathbf{n}$ $(p = 0)$ and otherwise of "oblique" rolls. In this latter case the symmetry is spontaneously broken with a 2-fold degeneracy, yielding "zig" and "zag" rolls with $p_{\mathrm{zig}} = -p_{\mathrm{zag}}$. The main control parameter is the amplitude of the applied voltage U_o, while the driving frequency $f = \omega/(2\pi)$ serves as a convenient second control parameter. Depending on the experimental conditions the direction of $\mathbf{q}$ may vary and in particular a wide range of possible wavelengths $\lambda = 2\pi/|\mathbf{q}|$ is available since $|\mathbf{q}|$ increases monotonously with the ac frequency f. At the so-called cut-off frequency f_c, which increases with decreasing charge relaxation time τ_q, the time symmetry of the modes changes [7,8]. In the low-frequency, *conductive* regime the director and the flow field are practically time independent, while the space charge distribution follows the external driving; in the high-frequency, *dielectric* regime the situation is reversed. In the following we will mostly focus on the conductive regime.

The theoretical understanding of the instability leading to EC patterns has been started with the seminal work of Carr [12] and Helfrich [13], who elucidated the basic positive feedback mechanism responsible for EC (now called the 'Carr–Helfrich (CH) mechanism' in the literature) in an approximate 1-d model. This approach has been later refined and generalized into a rigorous 3-d theory, the standard model (SM) [7,14].

The description of the electroconvecting state requires the knowledge of the velocity field $\mathbf{v}(\mathbf{r}, t)$, the director field $\mathbf{n}(\mathbf{r}, t)$ and the charge distribution $\rho_{\mathrm{el}}(\mathbf{r}, t)$ (or the electric potential $\phi(\mathbf{r}, t)$). These quantities may be calculated combining the highly nonlinear partial differential equations (PDEs) of nemato-hydrodynamics [3,7] with the quasi-static Maxwell-equations.

The equations governing the electric field $\mathbf{E}$ and the charge distribution ρ_{el} for a given $\mathbf{n}$ are

$$\nabla \cdot \mathbf{D} = \nabla \cdot (\boldsymbol{\epsilon}\mathbf{E} + \mathbf{P}_{\mathrm{flexo}}) = \rho_{\mathrm{el}}, \quad \nabla \cdot \mathbf{j} = \nabla \cdot (\boldsymbol{\sigma}\mathbf{E} + \rho_{\mathrm{el}}\mathbf{v}) = -\partial_t \rho_{\mathrm{el}}. \tag{1}$$

In contrast to isotropic materials the dielectric permittivity and the electrical conductivity become the tensors $\boldsymbol{\epsilon}$ and $\boldsymbol{\sigma}$, respectively. In the SM nematics are regarded as uniaxial dielectrics with a small ohmic conductivity, consequently

$$\epsilon_{ij} = \epsilon_\perp \delta_{ij} + \epsilon_a n_i n_j, \quad \sigma_{ij} = \sigma_\perp \delta_{ij} + \sigma_a n_i n_j. \tag{2}$$

Here ϵ_a and σ_a characterize the anisotropy of the nematic material. It is also noteworthy that in liquid crystals certain director distortions generate a flexoelectric polarization,

$$\mathbf{P}_{\mathrm{flexo}} = e_1 \mathbf{n}(\nabla \cdot \mathbf{n}) + e_3 (\mathbf{n} \cdot \nabla)\mathbf{n}, \tag{3}$$

with e_1 and e_3 known as the flexoelectric coefficients [3,4].

The essence of the CH mechanism is the following. Let us suppose a spatial fluctuation of $\mathbf{n}$ with a wavevector $\mathbf{q}$. Due to the anisotropy shown in Eq. (2) $\nabla \cdot \mathbf{j} = 0$ and $\nabla \cdot \mathbf{D} = 0$ cannot be fulfilled simultaneously if a spatial variation of $\mathbf{n}$ is present. Hence charge separation inevitably occurs in the electrically neutral LC yielding a spatially varying charge density ρ_{el}. The bulk force term $\rho_{\mathrm{el}}\mathbf{E}$ in the Navier–Stokes equation excites a flow field $\mathbf{v} \neq 0$ in form of vortices which build up a periodic roll pattern. The flow exerts a viscous torque on the director. If the amplitude of the original

fluctuation is enhanced (i.e. the feedback is positive), a macroscopic pattern evolves. Since viscous damping, the elastic and dielectric torques on **n** as well as charge diffusion act against the pattern forming CH mechanism, the onset of convection requires a finite voltage amplitude U_c which depends on ω and **q**.

The SM [14] which describes the EC mechanism is too complicated to be solved analytically together with realistic rigid boundary conditions (vanishing **v**, fixed **n** and ϕ at the confining plates). Hence investigations of EC typically start with a linear stability analysis of the homogeneous basic state, which yields (numerically) the threshold voltage $U_c(f)$ and the critical wavevector $\mathbf{q}_c(f)$ as a function of frequency. The results can be made more transparent by deriving approximate, though quite accurate analytical expressions for the critical quantities U_c and $\mathbf{q}_c$ [7]. Their inspection clearly demonstrates in which way various material parameters affect the efficiency of the CH mechanism. In particular it becomes obvious that a positive feedback requires certain combinations of the signs of the dielectric (ϵ_a) and of the conductivity (σ_a) anisotropies and of the symmetry of the configuration (planar or homeotropic alignment) [15]. Some of the possible combinations will be discussed in more detail in the following sections.

3. Anisotropic electroconvection (planar configuration, conventional material parameters)

We consider here the classical EC configuration; a planar nematic with $\sigma_a > 0$ and $\epsilon_a < 0$ (see Eq. (2)), a combination which further on will be referred to as the conventional material parameter set. This is the situation where EC was first observed and where most of the experimental and theoretical studies of past decades were focused on.

In the ground state the initial alignment is $\mathbf{n} = (1, 0, 0)$, i.e. the director is oriented along the x axis. The electric field **E** is perpendicular to **n**, so the dielectric torque stabilizes the ground state, i.e. the electric free energy density $f_{\mathrm{el}} = -\epsilon_0\epsilon_a(\mathbf{nE})^2/2$ is minimized. The electroconvection pattern develops when the applied electric voltage U exceeds the planar threshold U_c^{pl}. Fig. 1 depicts the characteristic properties of a normal roll pattern near onset in the conductive regime. In this case the director (indicated by double arrows) displays a periodic tilt distortion (with tilt angle θ) which is well described by the following components of **n**:

$$n_z(x, z, t) = \theta \sin(\mathbf{qx})\vartheta^{\mathrm{EC}}(q, z, t) \cong \theta \sin(\mathbf{qx}) \cos(\pi z/d); \quad n_x = 1 + \mathrm{O}(\theta^2); \quad n_y = 0 \tag{4}$$

with $\mathbf{x} = (x, y)$.

It follows from Eqs. (1) and (2) that positive charges (shown as +) are focussed at the locations with negative curvature of the director ($\partial_{xx} n_z < 0$) when the oscillating electric field points upwards. The resulting flow vortices (represented by the closed stream lines) generate a torque which produces a positive feedback increasing θ.

The situation shown in Fig. 1 corresponds to a *normal roll* pattern (i.e. **q** is parallel to the initial **n**). The splay-bend director distortion is restricted to the flow plane (x–z), which ensures the most efficient viscous torque (maximal coupling between flow **v** and **n**). Albeit this situation is optimal for the CH destabilization, it is also associated with maximal viscous dissipation. The dissipation diminishes if **q** rotates away from the x axis ($p \neq 0$, oblique rolls). Then the flow plane (being always parallel to **q**) does not coincide with the director distortion plane (x–z) anymore which involves a reduction of the destabilizing viscous torque. Oblique rolls thus represent a compromise: reduced viscous dissipation at the expense of less optimal coupling between flow and director.

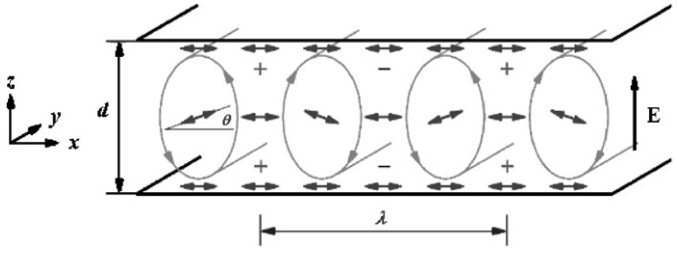

Fig. 1. Schematic representation of a planar EC roll pattern near onset with wavelength $\lambda = 2\pi/q$. θ is the tilt angle of the director (shown by double arrows), + and − label the charges and the elliptic closed stream lines indicate the convective flow.

Whether oblique rolls or normal rolls actually prevail at threshold is a subtle quantitative question, i.e. it depends on the material parameters of a specific nematic and the ac frequency f. The assessment of the critical voltage U_c^{pl} and the critical wave vector $\mathbf{q}_c$ at onset of convection from the numerical analysis of the SM compares very well with the experiments. If oblique rolls prevail, they appear at low frequencies f less than the Lifshitz frequency f_L.

The situation becomes more complicated in the nonlinear regime, where we restrict ourselves to the normal rolls. The primary bifurcation is supercritical, i.e. the tilt angle θ in Fig. 1 and the amplitude of the flow velocities grow continuously $\propto \sqrt{\varepsilon} = \sqrt{(U_0^2 - U_c^2)/U_c^2}$. It is intuitively clear that at too large tilt angles (say $\theta \gtrsim 45°$) the charge focusing mechanism becomes less effective (for the maximal distortion $\theta = 90°$ near the midplane there would be no charge separation at all).

The system can choose among various options to avoid too large θ. One is to generate oblique rolls in a secondary zig–zag (ZZ) bifurcation, which is observed typically at low frequencies ($f < f_{\mathrm{AR}}$). Alternatively the increase of θ with ε can also be reduced at fixed $\mathbf{q}$ by the excitation of director distortion modes homogeneous in the x–y plane but depending on z.

Typical is the director rotation out of the x–z plane by an azimuthal angle ϕ yielding a nonzero director component $n_y = \phi \cos(\pi z/d)$, while $\mathbf{q}$ remains parallel to the x axis. Thus in Fig. 1 the flow lines remain unmodified, while the director is rotated uniformly in the x–y plane ($n_y \neq 0$) resulting in a 3-d director deformation involving also twist. This configuration has been coined as *abnormal rolls*. The resulting phase diagram has been explored in great detail with particular focus on the vicinity of a codimension-2 point at f_{AR} separating oblique and abnormal rolls [16]. A set of amplitude equations which couple the amplitudes ($\propto \theta$) of the periodic roll modes with n_y have been constructed on the basis of general symmetry arguments [17] and their coefficients have been calculated rigorously from the equations of nematodynamics [18]. The detailed analysis of these equations, which cover also interesting modulated n_y structures up to complex defect-turbulent patterns [19–21], has contributed considerably to the understanding of the weakly-nonlinear EC regime.

One arrives for instance at the following expression for the growth rate σ of the n_y mode (of abnormal rolls):

$$\sigma = -T - Kk^2 + \Gamma|\theta|^2. \tag{5}$$

The constant damping term $-T$ is caused by the finite twist-elastic energy due to the z dependence of n_y (it has a maximum at the center plane, but is zero at the bounding electrodes). Slow modulations of n_y in the x–y plane with wavenumber $k \ll q_c$ are damped as well by the orientational elasticity (K). The abnormal roll instability is driven by the positive term $\Gamma\theta^2 \propto \varepsilon$ which enforces a sign change of σ for $k = 0$ at $\varepsilon = \varepsilon_{\mathrm{AR}}$, slightly above the primary EC bifurcation (obviously $\varepsilon_{\mathrm{AR}} \propto T/\Gamma$ and typically $\varepsilon_{\mathrm{AR}} \lesssim 0.1$). If ε increases further n_y grows and reacts on θ to block the further increase of n_z above its value at $\varepsilon_{\mathrm{AR}}$ [18,19].

It is obvious, that by the application of a magnetic field $\mathbf{H}$ parallel to $\mathbf{E}$ which exceeds the so called splay Freedericksz threshold field H_F a homogeneous tilt of $\mathbf{n}$ develops in the ground state. It is also intuitively clear that in this case the EC transition is pushed to larger voltages, since periodic distortions become harder to be excited (for details see e.g. [22]). It is interesting, that in some cases such a homogenous in-plane distortion is spontaneously excited (without $\mathbf{H}$), which also reduces the periodic distortion amplitude θ [23].

While earlier theoretical and experimental studies were typically focussed on the bifurcation scenarios occurring with increasing external driving, the present system has been shown recently to provide a good opportunity to investigate an 'adverse' scenario, namely the decay of an existing pattern [24]. In the following subsection it will be demonstrated that the resulting dynamics is far from trivial and yields additional insight into the parameter dependence of the director dynamics.

We should mention that, in addition to the standard EC roll patterns described above, in some cases patterns consisting of unusually wide stripes can be observed [5,25–27]. Just as in the standard normal roll case, the wide stripes are oriented perpendicular to the initial director orientation, but their wavelength is considerably larger ($\sim 4 - 6d$). Detection of the wide stripes requires crossed polarizers as they do not produce shadowgraph images at onset. Apparently, in some analogy to the abnormal rolls, n_y modulations are involved. Observations have shown that the flow stream lines, in contrast to Fig. 1, are confined to the x–y plane. The threshold voltage of the wide stripes has a weaker frequency dependence than either that of the conductive or that of the dielectric rolls. Consequently wide stripes usually appear as a crossover from a conductive (or a dielectric) roll pattern when increasing the ac frequency. Certainly the standard

CH mechanism (as shown in Fig. 1) does not apply for the wide stripes, but unfortunately at the moment a sustainable theoretical concept for their explanation is not available.

3.1. Decay of the regular patterns

We consider here a normal roll pattern with wavenumber q slightly above onset of EC (see Fig. 1). If the voltage is turned off suddenly, the pattern decays and the system returns to its equilibrium (homogeneous) state. The relaxation time τ characterizing the decay gives an important insight into the system dynamics. Thus we have made a systematic theoretical and experimental analysis of the decay process, focusing in particular on the wavenumber dependence of τ.

The theoretical analysis is based on the SM of EC, however, it becomes considerably simpler for two reasons. First, the decay occurs in the absence of an electric field, hence the relaxation of the director and of the flow are fully decoupled from that of the space charge distribution. Second, the amplitude of the director modulation becomes surely small during the decay (even if it was large at the beginning) so the remaining director and flow equations can safely be linearized. Finally one arrives at a linear, non-self-adjoint eigenvalue problem, which yields an infinite discrete spectrum of decay rates, $\mu_k(q)$ $(\mu_1 < \mu_2 < \cdots)$ [24], associated with the corresponding set of eigenmodes $N_k(q, z)$, which fulfill the orthonormality condition

$$\frac{\pi}{d}\int_{-d/2}^{+d/2} N_k(q,z)N_l^+(q,z)\,\mathrm{d}z = \delta_{kl}; \quad k,l = 1,2,\ldots\ . \tag{6}$$

Here $N_k^+(q, z)$ denotes the set of adjoint eigenmodes for the same $\mu_k(q)$ [28]; δ_{kl} is the Kronecker symbol.

Let us suppose that the EC director profile (characterized by the tilt $\vartheta^{\mathrm{EC}}(q, z, t)$) at the moment of voltage switch-off, which serves as the initial condition for the decay, is given as $\vartheta^{\mathrm{EC}}(q, z, 0) \ll 1$. From standard mathematics the subsequent temporal evolution can be represented as a linear superposition of the decaying modes $\theta_k^d(x, z, t) = e^{-\mu_k(q)t}\sin(qx)N_k(q, z)$ with weights $w_k(q)$ which are given as:

$$w_k(q) = \frac{\pi}{d}\int_{-d/2}^{+d/2} \vartheta^{\mathrm{EC}}(q,z,0)N_k^+(q,z)\,\mathrm{d}z; \quad k = 1,2,\ldots\ . \tag{7}$$

The dispersion relation curves $\mu_k(q)$ depend on the elastic moduli and on the viscosity coefficients of the nematic, and can be calculated numerically [24]. Fig. 2 exhibits the first few branches ($k = 1, \ldots, 7$) for the standard nematic EC substance Phase 5 (Merck).

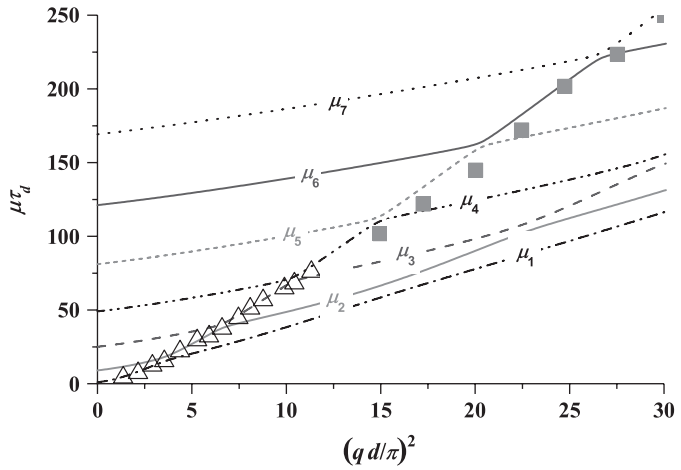

Fig. 2. Dependence of the relaxation rate on the wavenumber in dimensionless units for the first 7 decay eigenmodes (plotted with different line styles). τ_d is the director relaxation time. The symbols correspond to experimental relaxation rates μ_{expt} measured in Phase 5/5A (triangles for the conductive, squares for the dielectric regime).

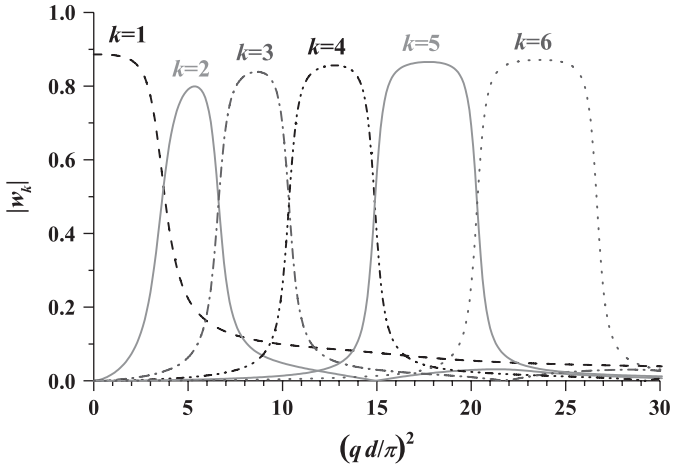

Fig. 3. Dependence of the weights of the first 6 decay eigenmodes on the dimensionless wavenumber of the roll pattern.

Laser diffraction at the optical grating due to the periodic director variation with wave vector **q** is a convenient technique for experimentally monitoring the decay of roll patterns and to compare with the theoretical predictions. The laser light after being transmitted through the cell creates a set of diffraction fringes on a screen. From their location the pattern wavelength and thus q can be determined, while their intensities are related to the pattern amplitude (the director distortion). Experiments have been carried out on planar samples of Phase 5 and Phase 5A using oblique light incidence. A fairly wide range of q, including both the conductive and the dielectric regimes, has been covered [24]. We concentrate for convenience on one of the first order diffraction fringes whose intensities, $I_{\pm1}(t)$, depend quadratically on the pattern amplitude (at small distortions) and thus reflect the pattern decay in time. After transients have died out the temporal evolution can be well fitted by a single exponential function $e^{-2t/\tau(q)}$ which defines our experimental value of the relaxation time $\tau(q)$ and the decay rate $\mu_{\text{expt}}(q)=1/\tau(q)$. Fig. 2 depicts some examples of μ_{expt} as symbols. Obviously they are closely related with one of the theoretical $\mu_k(q)$ curves; i.e. except some transition points we find for each q a certain $k=\bar{k}$ where $\mu_{\text{expt}}(q)=\mu_{\bar{k}}(q)$ holds. The index $\bar{k}$ increases monotonously with q.

The selection of a certain $\mu_{\bar{k}}$ for a given q is confirmed by the theoretical analysis. The weights $w_{\bar{k}}(q)$ calculated from Eq. (7) for a representative director profile $\vartheta^{\text{EC}}(q,z,t)$, which is known from a numerical solution of the SM, are plotted in Fig. 3. It is evident that the q axis can practically be covered by intervals $\mathcal{Q}_{\bar{k}}$ such that for $q\in\mathcal{Q}_{\bar{k}}$ the step-function-like curve $w_{\bar{k}}(q)$ dominates (e.g. $w_4(q)$ is dominant for $\mathcal{Q}_4=(10\lesssim(qd/\pi)^2\lesssim15)$). Consequently for $q\in\mathcal{Q}_{\bar{k}}$ the temporal evolution of the pattern is governed by the decay rate $\mu_{\bar{k}}(q)$. The contribution from eigenmodes other than the dominant one is negligible except at q values separating the neighboring intervals $\mathcal{Q}_{\bar{k}}$ and $\mathcal{Q}_{\bar{k}+1}$ [28].

As already discussed, the fringe intensity $I_{-1}(t)$ is mainly determined by the mode $N_{\bar{k}}(q,z)$ where the weight $w_{\bar{k}}(q)$ for a given $\vartheta^{\text{EC}}(q,z,0)$ is maximal. In addition the optical efficiency of a mode $N_k(q,z)$, which has been quantified by a factor $c_k^{\text{opt}}(q)$ in [28], has to be taken into account. Thus the temporal evolution of I_{-1} reads finally:

$$I_{-1}=\theta^2 C_q\left|\sum_{k=1}^{\infty}c_k^{\text{opt}}w_k e^{-\mu_k t}\right|^2. \tag{8}$$

To deal with the spatially varying refractive index of a roll pattern we have used a physical optics approach [29] to calculate the $c_k^{\text{opt}}(q)$ curves. They look very similar to the $w_k(q)$ curves in Fig. 3 as far as their q dependence is concerned. Since for a given q they show pronounced maxima for the same $\bar{k}$ the corresponding decay rate $\mu_{\bar{k}}$ dominates in Eq. (8) even more.

Inspection of Eq. (8) shows that with increasing time slower modes with $k<\bar{k}$ (with $\mu_k<\mu_{\bar{k}}$) should take over until the lowest branch μ_1 is reached in the long time limit. It has been checked, however, that this crossover (which is relevant for higher q where $\bar{k}>1$) cannot be resolved since the experimentally available time window is limited by acceptable signal-to-noise ratios and the resolution of the analog-to-digital converters.

According to our previous analysis the initial conditions have a strong influence on the system dynamics via the related mode selection mechanisms. If the director profile of the EC state differs considerably from that of the linear mode, decay eigenmodes with $k < \bar{k}$ (i.e. with slower decay) might be excited. Decay rates $\mu_k(q)$ with $k < \bar{k}$ could indeed be resolved experimentally at high q (in the dielectric regime) by altering the excitation voltage from sinusoidal to a pulsed square wave type [28].

4. Quasi-anisotropic electroconvection (homeotropic alignment, conventional material parameters)

In this situation, the director is oriented perpendicular to the confining plates ($\mathbf{n} = (0, 0, 1)$) and therefore the ground state is isotropic in the x–y plane. In case of conventional material parameters ($\sigma_a > 0$ and $\epsilon_a < 0$) the electric field (which is parallel to $\mathbf{n}$) is apparently destabilizing since $f_{\mathrm{el}} > 0$. This leads to a homogeneous director tilt towards the planar configuration for $U > U_F$ (bend Freedericksz transition) [3]. The tilt grows continuously with increasing U. The direction of the projection of the resulting $\mathbf{n}$ on the x–y plane is, however, not defined a priori but is singled out by the system in the Freedericksz transition at $U = U_F$. We describe this configuration, where the isotropy in the x–y plane is spontaneously broken, as 'quasi-anisotropic'. The selected tilt direction defines the x axis in the following.

Any spontaneously broken continuous symmetry is in general associated with a soft Goldstone mode, which tends to restore the symmetry. In the present case the Goldstone mode corresponds to a homogeneous rotation around the z axis ($n_y \neq 0$). The related growth rate is described by Eq. (5) with $T = 0$ (no damping at the boundary in contrast to the planar case) and $\theta = 0$.

When a sufficiently extended, nearly planar layer has developed near the midplane of the cell, the standard planar CH convection mechanism is activated at $U_c^h > U_F$ and one observes the pattern types familiar from the planar case. These considerations can be made more quantitative by introducing the average $\langle n_x \rangle$ of the x-component of the director along z as a measure of planarity which increases with increasing U. It turns out that $\langle n_x \rangle \gtrsim 0.5$ is already sufficient for the EC bifurcation to occur. We mention that the planar configuration discussed in Section 3 would formally correspond to $\langle n_x \rangle \approx 1$ with a critical voltage of U_c^{pl}. Then it is obvious from physical considerations that $U_c^h > U_c^{\mathrm{pl}}$ must hold for a conventional material parameter set.

The linear properties of the EC transition in the 'quasi-anisotropic' configuration have already been studied in detail [30,31]. One observes stationary normal or oblique rolls in good agreement with the theory. Recently travelling waves with a Hopf-frequency ω_H have also been detected and investigated at the threshold of EC [32]. Travelling rolls have been observed earlier in the planar geometry (Section 3) and been explained theoretically via a weak-electrolyte model (WEM) [33–35]. Though for the quasi-anisotropic situation such a detailed theoretical analysis is missing so far there is no doubt that WEM effects apply here as well. For instance the WEM scaling relation $\omega_H \propto d^{-3}\sigma_\perp^{-1/2}$ has been confirmed [32].

At $U > U_c^h$, the weakly nonlinear state of the quasi-anisotropic EC differs qualitatively from that of the planar convection. In analogy to the latter case, the periodic director tilt mode couples to the n_y (Goldstone) mode as in Eq. (5) but because of $T = 0$ the abnormal roll bifurcation appears already at $\varepsilon_{\mathrm{AR}} = 0$. Thus a direct transition to spatio-temporal chaos ("soft-mode turbulence") at onset appears in this system which has motivated detailed experimental and theoretical investigations in the past [36–40].

By the application of a magnetic field $\mathbf{H} = (H, 0, 0)$ normal to $\mathbf{E}$ an additional torque is exerted on the director which favors an orientation parallel to $\mathbf{H}$ where the magnetic free energy of $f_{\mathrm{magn}} = -\chi_a(\mathbf{n} \cdot \mathbf{H})^2$ would become minimal as the anisotropy of the magnetic susceptibility χ_a is usually positive. As a consequence the bend Freedericksz threshold voltage $U_F(H)$ decreases continuously with H reaching zero at the magnetic bend Freedericksz threshold field H_F. At finite H the degeneracy of the homeotropic orientation is lifted and thus the isotropy in the x–y plane is broken. $\mathbf{H}$ mimics the anchoring forces of the planar configuration since $T \propto H^2$ in Eq. (5). Thus it is not surprising that bifurcation scenarios familiar from the planar case are recovered.

It is worth noticing that wide stripe patterns, mentioned before in Section 3, are observable in the Freedericksz distorted quasi-planar homeotropic cells too (see Fig. 4 as an example). They have been called *prewavy* pattern (PW) [41] as they transform with increasing voltages into a wavy pattern containing undulated disclination lines. Recent experimental studies [42,43] have shown that the PW in homeotropic cells and the planar wide stripes have very similar characteristic properties which cannot be explained by the standard CH destabilization mechanism. This similarity is not surprising, since, as discussed before, quasi-anisotropic EC can be interpreted very well in terms of an effective

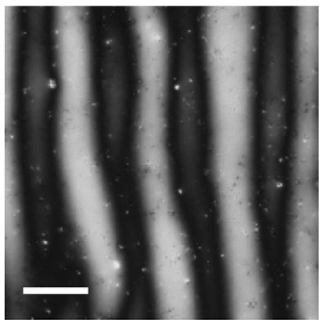

Fig. 4. Snapshot of a prewavy pattern (PW, $d = 50\,\mu$m) taken at crossed polarizers in N-(p-methoxybenzylidene)–butylaniline (MBBA). The director points in the horizontal direction. The white bar marks a distance of 250 μm.

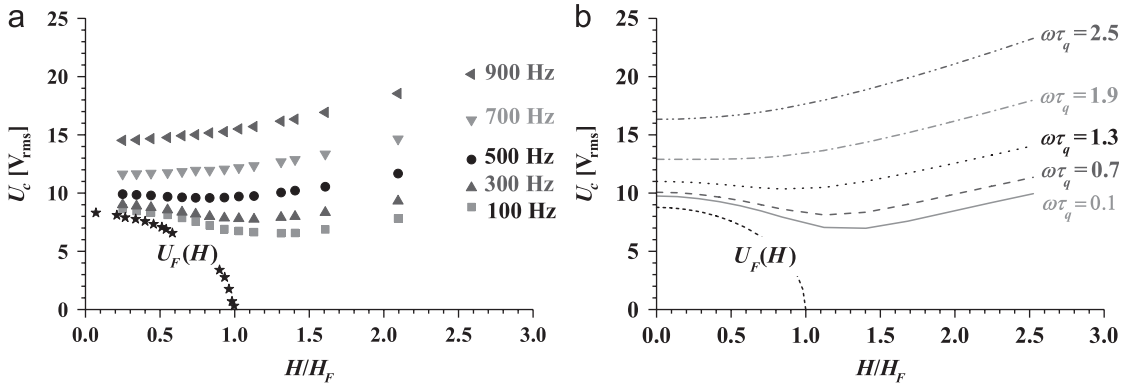

Fig. 5. Magnetic field dependence of the EC threshold voltages for various frequencies as well as that of the Freedericksz threshold voltage in the nematic Phase 5A. (a) Measured values, (b) curves calculated using the SM. Here $\tau_q = \epsilon_0\epsilon_\perp/\sigma_\perp$ is the charge relaxation time. $\omega\tau_q = 1$ roughly corresponds to the experimental frequency of 430 Hz.

planar layer. Thus the identification of the PW mechanism in the simpler planar case would most probably explain the homeotropic PW as well.

In the following subsections we first describe briefly the linear properties of EC in dependence on H. Then we turn to the nonlinear aspects before we discuss some very recent results on the dislocation dynamics.

4.1. Magnetic field effects on the threshold

In the case of finite H two opposite effects determine the critical voltage $U_c^h(H, f)$. Since the frequency independent $U_F(H)$ decreases with H, obviously the planarity of the Freedericksz state at a fixed U increases with H which is in favor of the EC onset. On the other hand the magnetic torque has a stabilizing effect on the resulting quasi-planar layer against the periodic splay-bend modulation characteristic of EC. As a rough measure for the latter (opposing) effect one can use the frequency dependent planar EC threshold $U_c^{\rm pl}(H, f)$ which increases monotonously with both H and f. Thus the ratio $U_c^{\rm pl}(H, f)/U_F(H) \equiv 1 + \beta$ increases with f as well as with H.

At low frequencies and not too large H we find a small β and the first effect prevails, such that $U_c^h(H, f)$ decreases as a function of H until a minimum, after which it increases steadily. At larger f, where β becomes larger, $U_c(H, f)$ increases monotonously for all H since the increased stiffness of the quasi-planar layer dominates. These general considerations are fully confirmed by detailed experimental studies [44,45] (see Fig. 5a) and theoretical simulations (see Fig. 5b) for the standard nematic Phase 5A.

The magnetic field also leads to morphological changes of the pattern which are manifested in the change of the roll obliqueness. It has already been reported earlier [45–48] that one finds in the quasi-anisotropic configuration for

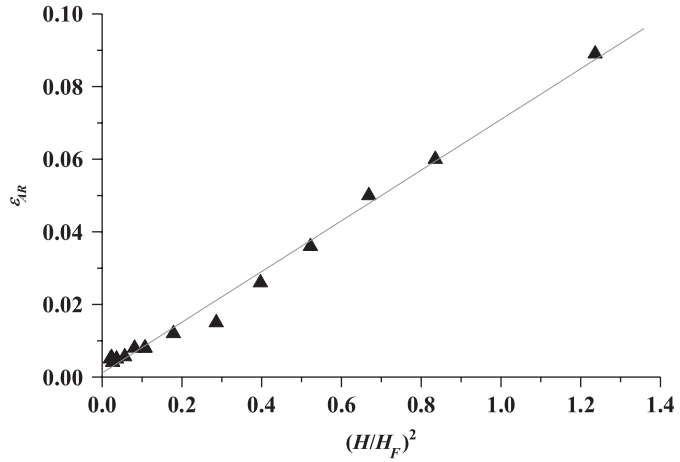

Fig. 6. Magnetic field dependence of the threshold $\varepsilon_{\mathrm{AR}}$ of the NR–AR transition in the nematic Phase 5A. Solid triangles are the measured values. The line corresponds to the power law fit $\varepsilon_{\mathrm{AR}} = 0.698(H/H_F)^2 + 0.001$.

the substance Phase 5A two Lifshitz points, i.e. oblique rolls can only be seen in a frequency range of $f_{L2} < f < f_{L1}$. Increasing the magnetic field results in a shift of the Lifshitz point(s) toward lower frequencies [44]. Consequently, at some H the lower Lifshitz point f_{L2} disappears and the usual behavior with a single Lifshitz point f_{L1} is recovered in good agreement with the theory.

4.2. Abnormal rolls

We have already pointed out in Section 4 that the azimuthal degeneracy of the director orientation at $H = 0$ leads to spatio-temporally chaotic patterns. They are characterized by variations of the azimuthal director angle φ as a manifestation of the underlying Goldstone mode. With increasing H that Goldstone mode is at first damped ($T \propto H^2$ in Eq. (5)) due to the magnetic torque on the director. However, with increasing tilt angle θ the damping is continuously reduced until in close analogy to the planar case the secondary normal roll (NR)–abnormal roll (AR) bifurcation takes place at $\varepsilon = \varepsilon_{\mathrm{AR}} \propto H^2$. It results in a homogeneous rotation (by an angle φ) of the director component in the x–y plane and thus of the optical axis while $\mathbf{q}$ remains unaltered. This transition is more easy to visualize optically in the homeotropic case than in the planar one, where according to Mauguin's principle [3] no twist deformation of the director can be detected in leading order.

The NR–AR transition is a forward pitchfork bifurcation. It has extensively been studied experimentally in the quasi-anisotropic configuration at fixed small magnetic fields [46–50]. The bifurcation has been explained theoretically using the formalism of amplitude equations where an excellent quantitative agreement between predicted and measured thresholds and azimuthal angles was obtained [46]. Our experimental set-up designed for the visualization and quantitative testing of abnormal rolls allowed to carry out the measurements at variable magnetic fields up to about $H \approx 2H_F$. It was found that for $H < H_F$ the predicted power law ($\varepsilon_{\mathrm{AR}} \propto H^2$) is confirmed (see Fig. 6) [44]. For large H, where certain approximations used for deriving the amplitude equations become invalid, the experimental $\varepsilon_{\mathrm{AR}}(H)$ saturates. The azimuthal angle of the director decreases with increasing H as expected due to the stabilizing torque of the magnetic field.

4.3. Dynamics of defects

Striped patterns generally are characterized by a certain stability regime ("Busse balloon" [1]) in the ε–$\mathbf{q}$ space. Even in the stable regime patterns have the tendency to reach an optimal wave vector $\mathbf{q}_{\mathrm{opt}}$ which coincides with $\mathbf{q}_c$ for not too large ε. During transients (e.g. immediately after changing the control parameters) patterns may exist whose actual $\mathbf{q}$ differs from the optimal one, i.e. a wavevector mismatch $\Delta\mathbf{q} = \mathbf{q} - \mathbf{q}_{\mathrm{opt}}$ is present. The formation and dynamics of dislocations offer an important possibility to adjust either the magnitude or the direction of the wavevector $\mathbf{q}$ in order

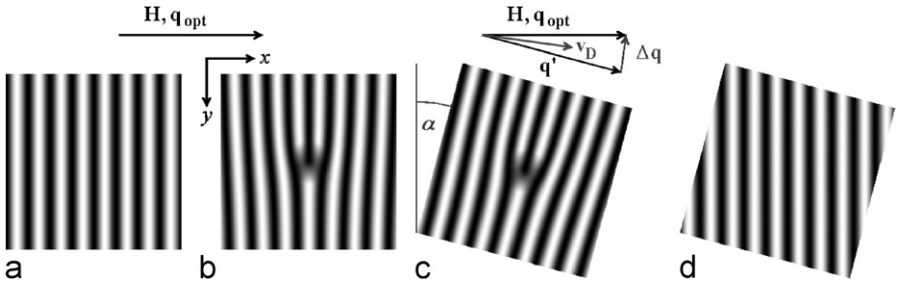

Fig. 7. Geometry of the defect motion measurements. (a) Initial pattern with $\mathbf{q} = \mathbf{q}_{\rm opt}$, (b) Pattern with a single defect, (c) Pattern immediately after rotation of the cell, (d) The stationary relaxed state.

to eliminate the mismatch. Dislocations are topological defects located at points where an additional roll ends in the bulk. The phase variation of the complex amplitude of the pattern around a dislocation defines the topological charge, with the possible values of ± 1 (the total phase variation divided by 2π). The defects move more smoothly parallel to the rolls ("climb") than perpendicular ("glide") since due to the translational invariance of a stripe pattern along the roll a climbing dislocation does not have to surmount additional energy barriers.

While the climb dynamics of dislocations changes the wavelength of the pattern (and so q), a glide motion alters the orientation of $\mathbf{q}$. The velocity $\mathbf{v}_D$ of the dislocations (magnitude and direction) depends on the wave vector mismatch $\Delta\mathbf{q}$. In the isotropic RBC near onset one has in certain cases (at large Prandtl number Pr) climb velocities $v_D \propto |\Delta\mathbf{q}|^{3/2}$ with a crossover to a $v_D \propto |\Delta\mathbf{q}|$ law at smaller Pr [51–53]. The situation is different and in some sense simpler in anisotropic planar EC [54]. Surprisingly climb and glide can be treated on the same basis, since the GL amplitude equation can be transformed into the isotropic Landau–Stewart equation while in isotropic RBC the anisotropic Newell–Whitehead equation applies [51].

The analysis of the GL equation predicts that for nonzero wavevector mismatch $\Delta\mathbf{q} = (\Delta q_x, \Delta q_y, 0)$ defects are expected to move perpendicular to $\Delta\mathbf{q}$ in a way that $|\Delta\mathbf{q}|$ decreases. The relation between the defect velocity $\mathbf{v}_D = (v_{Dx}, v_{Dy}, 0)$ and $\Delta\mathbf{q}$ becomes quite simple if the quantities are properly non-dimensionalized [54]:

$$\mathscr{V} ln(V_0/\mathscr{V}) = 2K(1 - 0.35K^2) \tag{9}$$

with the scaled velocity $\mathscr{V} = \frac{\tau_0}{\sqrt{\varepsilon}}\sqrt{v_{Dx}^2/\xi_\parallel^2 + v_{Dy}^2/\xi_\perp^2}$, mismatch $K = \frac{1}{\sqrt{\epsilon}}\sqrt{\Delta q_x^2\xi_\parallel^2 + \Delta q_y^2\xi_\perp^2}$, the coherence lengths $\xi_\parallel$, $\xi_\perp$, the correlation time τ_0 of the pattern and $V_0 = 3.29$. In particular the weak (logarithmic) nonanalyticity for $\Delta q \to 0$ [51,54,55] asks for experimental confirmation.

The first experimental test in EC in nematics was restricted to pure climb motion, by using sudden variations in the frequency f. Since q_c depends on f the pattern had to adjust the wavenumber and did so by climbing of dislocations [56]. The problem has been tackled again recently by focussing on the glide motion of defects in the quasi-anisotropic homeotropic configuration [57]. The idea is to produce a stationary, regular normal roll EC pattern with $\mathbf{q}_{\rm opt} = \mathbf{q}_c$ along x by applying a magnetic field $\mathbf{H}$ parallel to x (Fig. 7a). A defect (Fig. 7b) is then created in a controlled way by a laser beam and the cell is rotated by an angle α around the z axis, such that its actual wavevector $\mathbf{q}'$ (with $|\mathbf{q}'| = |\mathbf{q}_{\rm opt}|$) includes an angle α with the x axis (Fig. 7c); i.e. a mismatch $\Delta\mathbf{q} = \mathbf{q}' - \mathbf{q}_{\rm opt}$ is generated between the actual and the equilibrium wavevector directions. In order to eliminate this mismatch defects move (mainly glide) and the system relaxes to the state with $\mathbf{q} = \mathbf{q}_{\rm opt}$ (Fig. 7d).

The defect velocity, the coherence lengths and the correlation time of the pattern have been measured as a function of the rotation angle (mismatch) in the full Eckhaus stable range and an excellent agreement with the theoretical prediction of Eq. (9) has been achieved. Fig. 8 shows the final results which undoubtedly indicate the logarithmic singularity at $K = 0$. It was also shown that the defects move perpendicular to $\Delta\mathbf{q}$ as expected [57].

5. Isotropic electroconvection (homeotropic alignment, non-conventional material parameters)

The truly isotropic situation means on one hand the absence of any external anisotropy (preferred direction) in the x–y plane of the pattern which can easily be realized by having $\mathbf{n}$ parallel to $\mathbf{E}$ and the z axis like in the setup described

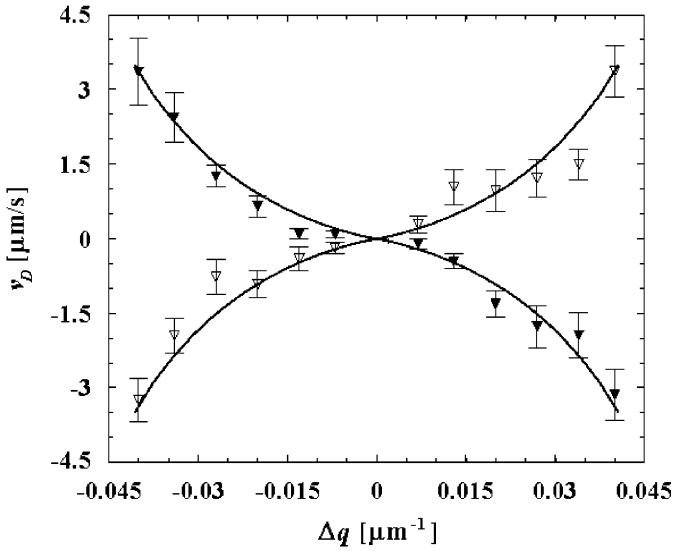

Fig. 8. Velocity of a single defect as the function of the wavevector mismatch Δq. Solid and open triangles, respectively, depict data measured for defects of opposite topological charge.

in Section 4. On the other hand one requires a direct transition from the homogeneous state into the patterned one without the intervening Freedericksz state. Thus one needs materials with $\epsilon_a > 0$. A closer look at the linear stability analysis shows that an EC destabilization of CH-type requires also $\sigma_a < 0$, which means the mobile charge carriers move preferentially perpendicular to the director. This looks counterintuitive, but in the vicinity of a nematic-smectic transition at which transport along $\boldsymbol{n}$ is eventually blocked by the generation of transverse layers, $\sigma_a < 0$ is easily achieved.

Recently a LC substance has been synthesized, that fulfills all the above requirements and thus is a successful candidate to produce a direct transition to (isotropic) EC. The material is a "swallow-tailed" compound, diethyl-6-[4-(4-(nitrobenzyloxy)-biphenyl-4′-oxy]hexylmalonate [58] which has a phase sequence: isotropic—110 °C—nematic—94 °C—smecticC—75 °C. EC measurements have been carried out at 96 °C in the nematic range [11,59,60].

Convection sets in directly from the undistorted ground state in a continuous transition i.e. the pattern amplitude grows gradually from zero. At low frequencies disordered rolls (stripes) are observed at threshold which consist of patches of oblique zig–zag rolls (see upper row of Fig. 9). Above a crossover frequency f_{sq} rolls are replaced by squares where the lines making up the squares are undulated ("*soft squares*") shown in the bottom row of Fig. 9. At frequencies slightly below f_{sq} a mixture of the two patterns, i.e. patches of rolls and squares, is observed.

Penetrating into the nonlinear regime (increasing the voltage above threshold) we observe in the zig–zag roll regime a persistent decrease of the size of regions with uniform roll orientation and an acceleration of the dynamics. The pattern looks eventually spatiotemporally chaotic, but without the point defects typical for anisotropic convection. In contrast, soft squares first undergo a transition into a crystal-like, rigid, almost perfect, quadratic or slightly rhombic lattice with sharp boundaries between differently oriented domains ("*hard squares*" shown in Fig. 10). The structure represents a quasiperiodic lattice spanned by more than two non-commensurate basic wave vectors. The coarsening of the hard square domains with time follows a power law $\sim t^{-\alpha}$ [61]. The measured growth exponent $\alpha = 0.5$ agrees well with the prediction for non-potential dynamics.

At first the onset of the EC patterns (behavior in the direct vicinity of the threshold) has been analyzed rigorously within the SM. The threshold voltage $U_c(f)$ as well as the critical wavevector $\mathbf{q}_c(f)$, match very well the experiments when fitting two particular viscosity parameters. They appeared to be much larger [59] than in standard nematics, but turned out to be very reasonable considering the vicinity of the smectic transition [62,63]. In a next step the weakly nonlinear regime was approached within an amplitude equation formalism. Using the parameters extracted from the linear analysis the calculated crossover frequency f_{sq} agreed almost perfectly with measurements. In addition the stability of the patterns in the weakly nonlinear regime was investigated. We found that both rolls and squares

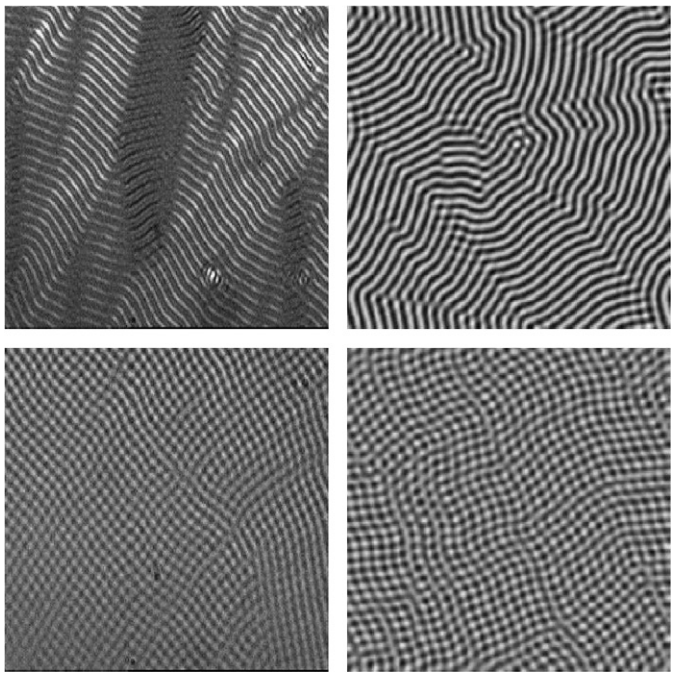

Fig. 9. Snapshots of *rolls* (above) and *soft squares* (below) in experiment (left) and simulation (right) for isotropic EC.

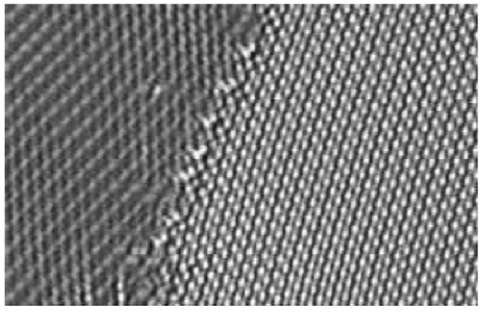

Fig. 10. Snapshot of *hard squares* for isotropic EC.

were unstable to modulational transverse modes (“zig–zag” instability), which are driven by strong mean flow effects. Surprisingly the zig–zag instability governs the whole wavevector band and not just the regime $q < q_c$ as in RBC.

To understand the steady, complex spatio-temporal state into which the patterns evolve under the zig–zag instability shown in Fig. 9 (left) and Fig. 10 in principle a full solution of the highly nonlinear nematodynamic equations would be required, which is inaccessible through the present computer capacities. We constructed a minimal model of the Swift–Hohenberg (SH) type, which is the standard approach to model isotropic pattern-forming systems in the weakly non-linear range. The model includes the coupling to the mean flow as well as certain terms to allow for the transition from rolls to squares. Results of numerical solutions of the SH equations are included into Figs. 9 and 11 (right), which reproduce nicely the experiments [11,60]. Particularly interesting is the long time evolution of the soft squares which settle (both in the experiment and theory) into an almost defect free, long-wave modulated, quasi-periodic square pattern shown in Fig. 11.

It is obvious that isotropic EC has several attractive novel aspects which deserve further studies. In contrast to the well understood usual competition of rolls and hexagons (e.g. in isotropic RBC), here the competition between rolls and squares can be systematically investigated in the same large-aspect ratio cell (about 2000 rolls) just by changing the

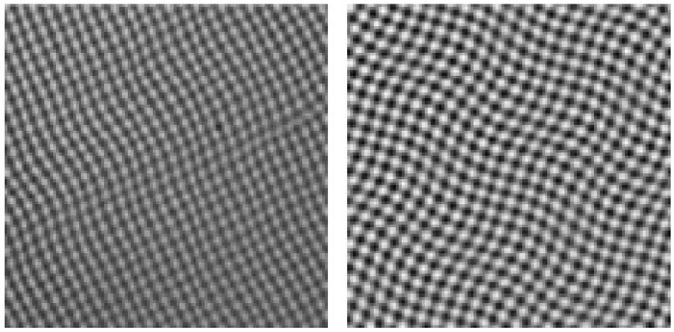

Fig. 11. Snapshot of long wavelength modulated, quasi-periodic square pattern for isotropic EC. Experiment (left) and simulation (right).

frequency. While rolls are disordered by a zig–zag modulation, squares suffer a long wavelength undulation. The soft squares settle into a static, spatially quasi-periodic attractor. Some quantitative details, and in particular the transition from soft to hard squares, demand future work. A particularly intriguing feature is the impact of mean flow. Usually it is responsible for complex dynamics like spiral defect chaos [2], however, here it leads to a very mild form of disorder or even to the generation of unconventionally ordered patterns. Our expectation is that similar structures might arise in other systems provided the aspect ratio can be made comparably large.

6. Nonstandard electroconvection (planar alignment with material parameters which exclude the standard mechanism)

Standard EC (s-EC, based on the *Carr–Helfrich* mechanism) is excluded according to the SM for the material parameter combination $\epsilon_a < 0$ and $\sigma_a < 0$ both in the conductive and in the dielectric regimes [15]. Nevertheless convection associated with roll formation in an ac electric field has been observed in several such compounds, e.g. in the homologous series of N-(p-n–alkyloxy–benzylidene)-n-alkyl-anilines, di-n-4-4′-alkyloxy–azoxy–benzenes and 4-n-alkyloxy–phenyl–4-n'alkyloxy–benzoates [64–66]. Fig. 12 shows a typical example of such patterns. The characteristics of the patterns like frequency dependence of the wavevector and of the critical voltage, the director dynamics in space and time, the optical contrast, etc., are different from those of the s-EC. Since this roll formation process falls outside the frame of the standard model it has been called nonstandard electroconvection (ns-EC).

The main experimental characteristics of the ns-EC patterns which differ from those of s-EC are:

- The overall contrast is low. The pattern near onset cannot be visualized by conventional shadowgraph imaging, instead crossed polarizers are needed to detect it.
- The contrast does not exhibit a sharp increase at onset, instead it grows rather gradually with the voltage. In addition one observes flow dynamics before the genuine ns-EC patterns become detectable.
- The pattern remains stable above threshold over an unusually broad voltage range up to the appearance of the turbulent states which are then visible as standard shadowgraph images.
- The threshold voltage scales with the cell thickness, thus the ns-EC onset is characterized by a critical electric field.
- The threshold voltage is a linear function of the driving ac frequency.
- In contrast to s-EC the critical wavevector is perpendicular to or includes a large angle with the basic director alignment. Thus one speaks of longitudinal rolls (or parallel stripes, PS) or strongly oblique rolls.
- The critical wavelength does not scale with the cell thickness.
- The pattern is less regular (see Fig. 12) due to spatial variations of $\mathbf{q}$ which presumably indicate a quite weak dependence of the critical voltage on q (i.e. a shallow neutral surface).

Several possible mechanisms for ns-EC have been proposed in the literature: a hand-waving argument based on "destabilization of twist fluctuations" [64], a speculation on an isotropic mechanism (based on the non-uniform space charge distribution along the field [65]) and the flexoelectric effect [67–69], but none of them has been analyzed in detail enough to show that they are capable to explain all features of the ns-EC patterns.

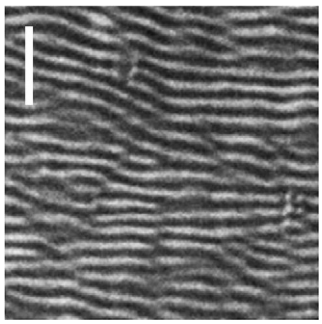

Fig. 12. Snapshot of longitudinal rolls (parallel stripes, PS, $d = 11\,\mu m$) taken at crossed polarizers in the nematic 4-*n*-octyloxy-phenyl-4-*n*′-heptyloxy-benzoate (**8/7**). The director is horizontal. The white bar marks a distance of 100 μm.

There are, however, at least some indications, that the flexoelectric polarization (see Eq. (3)) is an important ingredient to understand ns-EC. To support this idea we have made a comparison with the static flexoelectric domains, observed in some experiments in the case of dc or very low frequency ac voltages [69]. These patterns bear some remarkable similarity to ns-EC patterns as far as the orientation of the **q** vector is concerned. The flexoelectric domains can be described within the standard model by incorporating flexoelectricity but neglecting flow and conductivity, i.e. only the director degrees of freedom are involved in the calculations [4,65]. In fact one can find a solution of the basic equations where the director is spatially periodic along the y axis. It turns out that the critical voltage of the flexoelectric domains depends on the flexoelectric coefficients like $|e_1 - e_3|^{-1}$ and can become arbitrarily small for large $|e_1 - e_3|$. On the other hand in the limit of vanishing flexoelectricity or if e_1 and e_3 do not differ much, the threshold of the flexoelectric domains would diverge.

The theoretical analysis can be generalized by the inclusion of the flow field and a finite electrical conductivity. In case of $\sigma_a > 0$ one recovers a standard EC scenario with conductive and dielectric regimes, where the influence of flexoelectricity rapidly vanishes with the frequency [70]. In our case (where $\sigma_a < 0$), however, surprisingly we do find a bifurcation to an EC pattern owing to flexoelectricity with strongly oblique (nearly parallel) rolls with the dielectric time symmetry even for low f [71]. The existence of the static flexoelectric domains in the flowless case is a valuable indicator for such an EC solution at finite f. Thus the qualitative dependence of EC pattern characteristics on the flexoelectric coefficients is similar to those in the flow less case, however, there are considerable quantitative changes which are consistent with the experiments: e.g. the wave vector of the rolls rotates out of the y direction and at finite frequency the onset voltage and the critical wavenumber are considerably reduced compared to the convection free flexoelectric domain state. The detailed analysis is still under progress, as it requires a fitting of the flexoelectric coefficients, which are difficult to measure. Nevertheless the first preliminary results look promising.

7. Electroconvection in a banana nematic

All nematics mentioned so far are composed of elongated, rod-like molecules. Recently a new class of liquid crystalline materials has been discovered; substances with bent-core (banana shape) molecules. They present a vast variety of new phases, not seen in the standard LCs, among them ferroelectric and biaxial nematic ones, which have become targets of intense investigations (for a recent review see [72,73] and references therein). Some of those ‘banana’ phases (e.g. the so-called B2 and B7) represent a polar order of the molecules. A conventional (uniaxial) nematic phase may also be found in some bent-core mesogens. There are speculations, that a short range polar ordering of their molecules might exist even in this nematic phase which could yield some unusual physical properties. However, experimental studies are just at the beginning and are certainly insufficient so far to establish relations between molecular ordering and material parameters.

In the previous sections it has been convincingly demonstrated that EC is an excellent tool to explore the physics of LCs. Thus it was natural to explore whether EC exists in banana nematics. In the present section we refer to the most detailed investigation [74] on a well characterized, planarly aligned bent-core nematic substance 4-chloro-1,3-phenylene bis 4-[4′-(9-decenyloxy) benzoyloxy] benzoate (ClPbis10BB) [74–76]. This substance has a giant

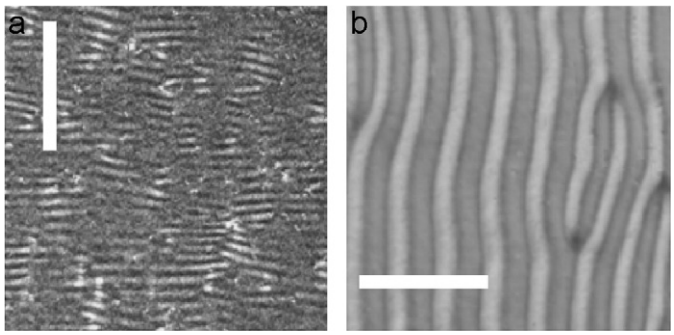

Fig. 13. Snapshots of (a) parallel stripes (PS, $d = 15\,\mu m$), (b) prewavy pattern (PW1, $d = 10\,\mu m$) taken at crossed polarizers in the banana nematic ClPbis10BB. The director is horizontal. The white bars mark a distance of 100 μm.

flexoelectric coefficient e_3 [77] and a large rotational viscosity. Another unusual feature is the small ($|\sigma_a/\sigma_\perp| < 0.22$) and frequency dependent anisotropy of the electrical conductivity characterized by a double sign inversion; $\sigma_a < 0$ at low ac frequency $f < 1.5$ kHz as well as at high $f > 8$ kHz frequencies, whereas $\sigma_a > 0$ for a fairly small (1.5 kHz $< f <$ 8 kHz) window. On the other hand $\epsilon_a < 0$ holds up to $f \approx 100$ kHz. Based on the morphology of the patterns four distinct frequency ranges could be distinguished [74]. At very low frequencies ($f < f_1 \approx 28$ Hz) a pattern of parallel stripes (PS) has been observed (Fig. 13a) which shows features very similar to the longitudinal rolls described before in Section 6 and shown in Fig. 12. At $f = f_1$ there is a crossover to a different stripe pattern running normal to **n** (PW2) and characterized by a large wavelength (some multiple of d). These wide stripes persist up to $f_2 = 1$ kHz, but reappear again (PW1) at large frequencies ($f > f_3 = 5$ kHz) thus straddling a frequency range ($f_2 < f < f_3$) where no pattern was detected.

The PW1 and PW2 patterns (for a representative example see Fig. 13b) and the wide-stripe (prewavy) patterns in standard rod-like nematics [25–27,41–43] (briefly addressed in Sections 3 and 4) look quite similar, they are only visible with crossed polarizers. In the standard materials (where $\sigma_a > 0$, $\epsilon_a < 0$) the PW are, however, an exception and the system chooses almost exclusively the alternative option of s-EC driven by the standard CH mechanism. The situation is different for the banana nematic. In the whole frequency range ($f_1 < f < f_2$) where the PW2 exists s-EC is excluded a priori in our planar geometry since $\sigma_a < 0$, $\epsilon_a < 0$ holds. On the other hand the PW1 exists in a frequency range ($f > f_3 = 5$ kHz), which contains also the window ($f_3 < f <$ 8 kHz) where $\sigma_a > 0$, $\epsilon_a < 0$ though s-EC has not been observed so far. As a consequence we tend to conclude that the sign of σ_a does not play a crucial role for the existence of PW patterns. Other differences between PWs in the standard and our banana nematics look more spectacular. First the growth and decay rates in the latter case are very low (several hours compared to seconds in standard nematics). Secondly the threshold voltages of both the PW2 and the PW1 prewavy modes diverge when approaching either f_2 from below (PW2) or f_3 from above (PW1).

The parallel stripes (PS) observed in standard and in banana nematics share more properties. Both need crossed polarizers for their observation and seem to exist only for the parameter combination $\sigma_a < 0$, $\epsilon_a < 0$.

In this section we have discussed two nonstandard EC pattern species (PW and PS) both visible with crossed polarizers, which cannot be explained by the CH destabilization mechanism. Since PW and PS differ in almost all other characteristics (e.g. in the magnitude and direction of $\boldsymbol{q}_c$ as function of f) one needs most probably two different models for their description, which remains as a challenge for future work.

8. Conclusions

In this paper we have demonstrated that depending on the sign of the electric anisotropies and on the initial director orientation, either anisotropic or isotropic electroconvection is observed in nematics. These scenarios are well understood in terms of the Carr–Helfrich destabilization mechanism (a positive feedback loop between director distortion, charge separation and flow) and thus can well be described theoretically by the standard model of electroconvection. We have mainly focussed on some recent studies which convincingly demonstrate the good agreement between experiment and theory in quite different situations.

We have also reported on nonstandard electroconvection patterns, like parallel stripes and prewavy pattern, in rod-like as well as in bent-core nematics with material parameter combinations where the CH destabilization mechanism does not work. Their understanding requires the inclusion of new (up to now neglected) mechanisms/phenomena into the standard model of EC (e.g. flexoelectricity, drift-recombination induced boundary layers, WEM, etc.). There are indications that flexoelectricity, which can cause an additional charge separation mechanism upon director distortions, may play a crucial role in the explanation of some ns-EC patterns.

An improvement/extension of the theoretical description would be important also from the point of view of transferring knowledge obtained on EC to other, less studied systems. For example the concepts of nematodynamics have recently found their way to biophysics too. In fact the interaction of biopolymers with active elements can lead to specific patterns with nematic ordering [78].

Acknowledgment

The authors are grateful to A. Krekhov and T. Tóth Katona for valuable discussions. This work was supported by the EU network PHYNECS (EU-HPRN-CT-2002-00312), and the Hungarian Research Funds OTKA T-037336, OTKA K-61075.

References

[1] M.C. Cross, P.C. Hohenberg, Rev. Mod. Phys. 65 (1993) 851.
[2] E. Bodenschatz, W. Pesch, G. Ahlers, Annu. Rev. Fluid Mech. 32 (2000) 709.
[3] P.G. de Gennes, J. Prost, The Physics of Liquid Crystals, Clarendon Press, Oxford, 1993.
[4] S.A. Pikin, Structural Transformations in Liquid Crystals, Gordon and Breach, New York, 1991.
[5] L.M. Blinov, V.G. Chigrinov, Electrooptic Effects in Liquid Crystal Materials, Springer, New York, 1994.
[6] A. Buka, L. Kramer (Eds.), Pattern Formation in Liquid Crystals, Springer, New York, 1996.
[7] L. Kramer, W. Pesch, in: A. Buka, L. Kramer (Eds.), Pattern Formation in Liquid Crystals, Springer, New York, 1996, p. 221.
[8] L. Kramer, W. Pesch, in: D.A. Dunmur, A. Fukuda, G.R. Luckhurst (Eds.), Physical Properties of Liquid Crystals: Nematics, Inspec, London, 2001, p. 441.
[9] W. Pesch, U. Behn, in: F.H. Busse, S.C. Mueller (Eds.), Evolution of Spontaneous Structures in Dissipative Continuous Systems, Springer, New York, 1998, p. 335.
[10] W. Pesch, L. Kramer, in: A. Buka, L. Kramer (Eds.), Pattern Formation in Liquid Crystals, Springer, New York, 1996, p. 69.
[11] Á Buka, B. Dressel, L. Kramer, W. Pesch, Phys. Rev. Lett. 93 (2004) 044502.
[12] E.F. Carr, Mol. Cryst. Liq. Cryst. 7 (1969) 253.
[13] W. Helfrich, J. Chem. Phys. 51 (1969) 4092.
[14] E. Bodenschatz, W. Zimmermann, L. Kramer, J. Phys. (Paris) 49 (1988) 1875.
[15] Á Buka, N. Éber, W. Pesch, L. Kramer, in: A.A. Golovin, A.A. Nepomnyashchy (Eds.), Self-Assembly, Pattern Formation and Growth Phenomena in Nano-Systems, NATO Science Series II, Mathematica, Physics and Chemistry, vol. 218, Springer, Dordrecht, 2006, p. 55.
[16] For a review see L. Kramer, B. Dressel, H. Zhao, W. Pesch, Mol. Cryst. Liq. Cryst. 368 (2000) 101 and references therein.
[17] E. Plaut, W. Decker, A.G. Rossberg, L. Kramer, W. Pesch, A. Belaidi, R. Ribotta, Phys. Rev. Lett. 79 (1997) 2367.
[18] E. Plaut, W. Pesch, Phys. Rev. E 59 (1999) 1747.
[19] A.G. Rossberg, A. Hertrich, L. Kramer, W. Pesch, Phys. Rev. Lett. 76 (1996) 4729.
[20] H. Zhao, L. Kramer, Phys. Rev. E 62 (2000) 5092.
[21] S. Komineas, H. Zhao, L. Kramer, Phys. Rev. E 67 (2003) 031701.
[22] J.T. Gleeson, Phys. Rev. E 54 (1996) 6424.
[23] B. Dressel, L. Pastur, W. Pesch, E. Plaut, R. Ribotta, Phys. Rev. Lett. 88 (2002) 024503.
[24] N. Éber, S.A. Rozanski, Sz. Németh, Á Buka, W. Pesch, L. Kramer, Phys. Rev. E 70 (2004) 061706.
[25] P. Petrescu, M. Giurgea, Phys. Lett. 59A (1976) 41.
[26] A.N. Trufanov, M.I. Barnik, L.M. Blinov, in: L. Bata (Ed.), Advances in Liquid Crystal Research and Application, Akadémiai Kiadó Budapest, Pergamon Press, New York, 1980, p. 549.
[27] L. Nasta, A. Lupu, Mol. Cryst. Liq. Cryst. 71 (1981) 65.
[28] W. Pesch, L. Kramer, N. Éber, Á Buka, Phys. Rev. E 73 (2006) 061705.
[29] H.M. Zenginoglou, J.A. Kosmopoulos, J. Opt. Soc. Am. A 14 (1997) 669.
[30] A. Hertrich, W. Decker, W. Pesch, L. Kramer, Phys. Rev. E 58 (1998) 7355.
[31] H. Richter, N. Kloepper, A. Hertrich, Á Buka, Europhys. Lett. 30 (1995) 37.
[32] S.-Q. Zhou, N. Éber, Á Buka, W. Pesch, G. Ahlers, Phys. Rev. E 74 (2006) 046211.
[33] M. Treiber, L. Kramer, Phys. Rev. E 58 (1989) 1973.
[34] M. Treiber, L. Kramer, Mol. Cryst. Liq. Cryst. 261 (1995) 951.
[35] M. Treiber, N. Éber, Á Buka, L. Kramer, J. Phys. II (Paris) 7 (1997) 649.

[36] S. Kai, K. Hayashi, Y. Hidaka, J. Phys. Chem. 100 (1996) 19007.
[37] Y. Hidaka, J.-H. Huh, K. Hayashi, M. Tribelsky, S. Kai, J. Phys. Soc. Jpn. 66 (1997) 3329.
[38] P. Toth, Á Buka, J. Peinke, L. Kramer, Phys. Rev. E 58 (1998) 1983.
[39] A.G. Rossberg, A. Hertrich, L. Kramer, W. Pesch, Phys. Rev. Lett. 76 (1996) 4729.
[40] A.G. Rossberg, L. Kramer, Phys. Scr. T 67 (1996) 121.
[41] S. Kai, K. Hirakawa, Solid State Commun. 18 (1976) 1573.
[42] J.-H. Huh, Y. Hidaka, Y. Yusuf, N. Éber, T. Tóth-Katona, Á Buka, S. Kai, Mol. Cryst. Liq. Cryst. 364 (2001) 111.
[43] J.-H. Huh, Y. Yusuf, Y. Hidaka, S. Kai, Mol. Cryst. Liq. Cryst. 410 (2004) 39.
[44] N. Éber, Sz. Németh, A.G. Rossberg, L. Kramer, Á Buka, Phys. Rev. E 66 (2002) 036213.
[45] N. Éber, Á Buka, Phase Trans. 78 (2005) 433.
[46] A.G. Rossberg, N. Éber, Á Buka, L. Kramer, Phys. Rev. E 61 (2000) R25.
[47] Á Buka, P. Tóth, N. Éber, L. Kramer, Phys. Rep. 337 (2000) 157.
[48] N. Éber, A.G. Rossberg, Á Buka, L. Kramer, Mol. Cryst. Liq. Cryst. 351 (2000) 161.
[49] H. Richter, Á Buka, I. Rehberg, Phys. Rev. E 51 (1995) 5886.
[50] J.-H. Huh, Y. Hidaka, S. Kai, Phys. Rev. E 58 (1998) 7355.
[51] For a comprehensive discussion see, L.M. Pismen, Vortices in Nonlinear Fields, Clarendon Press, Oxford, 1999.
[52] G. Tesauro, M.C. Cross, Phys. Rev. A 34 (1986) 1363.
[53] Th. Walter, W. Pesch, E. Bodenschatz, Chaos 14 (2004) 933.
[54] E. Bodenschatz, W. Pesch, L. Kramer, Physica D 32 (1988) 135.
[55] E. Bodenschatz, A. Weber, L. Kramer, J. Stat. Phys. 64 (1991) 1007.
[56] S. Rasenat, V. Steinberg, I. Rehberg, Phys. Rev. A 42 (1990) 5998.
[57] P. Toth, N. Éber, T.M. Bock, Á Buka, L. Kramer, Europhys. Lett. 57 (2002) 824.
[58] U. Emmerling, S. Diele, H. Schmalfuss, J. Werner, H. Kresse, J. Lindau, Macromol. Chem. Phys. 199 (1998) 1529.
[59] Á Buka, B. Dressel, W. Otowski, K. Camara, T. Tóth-Katona, L. Kramer, J. Lindau, G. Pelzl, W. Pesch, Phys. Rev. E 66 (2002) 051713.
[60] Á Buka, B. Dressel, L. Kramer, W. Pesch, Chaos 14 (2004) 793.
[61] E. Kochowska, N. Éber, W. Otowski, Á Buka, Mol. Cryst. Liq. Cryst. 435 (2005) 243.
[62] H. Kneppe, F. Schneider, N.K. Sharma, J. Chem. Phys. 77 (1981) 3203.
[63] L. Bennett, S. Hess, Phys. Rev. E 60 (1999) 5561.
[64] M. Goscianski, L. Leger, J. Phys. (Paris) 36 (1975) C1-231.
[65] L.M. Blinov, M.I. Barnik, V.T. Lazareva, A.N. Trufanov, J. Phys. (Paris) 40 (1979) C3-263.
[66] E. Kochowska, S. Németh, G. Pelzl, Á Buka, Phys. Rev. E 70 (2004) 011711.
[67] N.V. Madhusudana, V.A. Raghunathan, Mol. Cryst. Liq. Cryst. Lett. 5 (1988) 201.
[68] N.V. Madhusudana, V.A. Raghunathan, Liq. Cryst. 5 (1989) 1789.
[69] M.I. Barnik, L.M. Blinov, A.N. Trufanov, B.A. Umanski, J. Phys. (Paris) 39 (1978) 417.
[70] W. Thom, W. Zimmermann, L. Kramer, Liq. Cryst. 4 (1989) 309.
[71] A. Krekhov, private communication.
[72] H. Takezoe, Y. Takanishi, Jap. J. Appl. Phys. 45 (2006) 597.
[73] T.C. Lubensky, L. Radzihovsky, Phys. Rev. E 66 (2002) 031704.
[74] D.B. Wiant, J.T. Gleeson, N. Éber, K. Fodor-Csorba, A. Jákli, T. Toth-Katona, Phys. Rev. E 72 (2005) 041712.
[75] K. Fodor-Csorba, A. Vajda, G. Galli, A. Jákli, D. Demus, S. Holly, E. Gács-Baitz, Macromol. Chem. Phys. 203 (2002) 1556.
[76] D. Wiant, S. Stojadinovic, K. Neupane, S. Sharma, K. Fodor-Csorba, A. Jákli, J.T. Gleeson, S. Sprunt, Phys. Rev. E 73 (2006) 030703.
[77] J. Harden, B. Mbanga, N. Éber, K. Fodor-Csorba, S. Sprunt, J.T. Gleeson, A. Jákli, Phys. Rev. Lett. 97 (2006) 157802.
[78] K. Kruse, J.F. Joanny, F. Jülicher, J. Prost, K. Sekimoto, Phys. Rev. Lett. 92 (2004) 078101.